NASA Technical Memorandum 105259

An Iterative Implicit Diagonally-Dominant Factorization Algorithm for Solving the Navier-Stokes Equations

Shu-Cheng Chen, Nan-Suey Liu and Hyun Dae Kim
Lewis Research Center
Cleveland, Ohio

October 1991

NASA

An Iterative Implicit Diagonally-Dominant Factorization Algorithm For Solving the Navier-Stokes Equations

Shu-Cheng Chen, Nan-Suey Liu and Hyun Dae Kim

National Aeronautics and Space Administration
Lewis Research Center
Cleveland, Ohio 44135

Abstract

This paper presents an algorithm for solving the multi-dimensional unsteady Navier-Stokes equations for compressible flows. It is based on a diagonally-dominant approximate factorization procedure. The factorization error and the timewise linearization error associated with this procedure are reduced by performing Newton-type inner iterations at each time step. The inviscid fluxes are evaluated by the fourth-order central differencing scheme amended with a numerical dissipation directly proportional to the entire dissipative part of the truncation error intrinsic to the third-order-biased upwind scheme. The important features of the proposed solution algorithm and the finite-difference scheme are elucidated by the numerical results of the convection of a vortex and the backward-facing step flows.

1. Introduction

In the past, both upwind and central differencing schemes have been used in the solution algorithms for the Navier-Stokes equations. These two approaches have their relative merits and shortcomings. One of the objectives of the present effort is to find a scheme that combines the merits of both central differencing and upwind differencing schemes. Another objective is to construct a multi-dimensional solution algorithm which is not only time-accurate but also robust with respect to this new differencing scheme.

In this work, the development of such an algorithm is based upon a Diagonally-Dominant Alternating-Direction-Implicit (DDADI) approximate factorization procedure [1] in conjunction with a Newton-type iterative process [2] for implicitly advancing the solution from one time level to the next. A description of this solution algorithm is given in Section 2. In Section 3, it is shown that the proposed difference scheme can be characterized as a fourth-order central differencing scheme with its added dissipation being consistent with the numerical dissipation intrinsic to the third-order-biased upwind scheme, and is termed here as the FCTD differencing scheme (Fourth-order Central with Truncation-error-type Dissipation).

The convection of an inviscid vortex in free stream has been used to study the performances of the proposed algorithm/scheme. Some selected results of this test case are presented in Section 4. To demonstrate its applicability for the viscous flows, the proposed algorithm/scheme has also been used to calculate the flows over a backward-facing step. The comparisons between the calculated results and the corresponding experimental data are shown in Section 5. The stability characteristics of

the proposed algorithm/scheme when applied to a three-dimensional domain are described in the Appendix.

2. The Iterative Implicit Diagonally-Dominant Approximate Factorization

This is the overall algorithm for solving the unsteady multi-dimensional compressible Navier-Stokes equations. To describe this algorithm, we consider the two-dimensional Navier-Stokes equations written in generalized coordinates (ξ, η),

$$\frac{\partial \hat{Q}}{\partial \tau} + \frac{\partial}{\partial \xi}\left(\hat{E} - \hat{E}_v\right) + \frac{\partial}{\partial \eta}\left(\hat{F} - \hat{F}_v\right) = 0 \qquad (1)$$

where $\hat{Q} = Q/J$; $Q = (\rho, \rho u, \rho v, e)^T$, and $J = \xi_x \eta_y - \xi_y \eta_x$ is the metric Jacobian. Here, τ is the time; ρ is the fluid density; e is the total internal energy per unit volume; u and v are the velocity components in the x and y directions of a Cartesian coordinates system. The transformed inviscid fluxes are denoted by $\hat{E}$ and $\hat{F}$; and the transformed viscous fluxes are denoted by $\hat{E}_V$ and $\hat{F}_V$. The specific forms of these transformed fluxes are well known and will not be repeated here.

To advance the solution of Eq. (1) from the n-th time level to the (n+1)-th level, the iterative implicit technique of Ref.[2] is adopted. Furthermore, the three-point backward time differencing is used to attain the second-order temporal accuracy. Let

$$(\delta f)^{(l)} = f^{(l+1)} - f^{(l)}, \qquad l = 1,2,3,\cdots m \qquad (2)$$

$$\left(\hat{Q}\right)^{(l)} = \hat{Q}^{(n)}, \qquad l=1 \tag{3}$$

$$\sum_{l=1}^{m} \left(\delta\hat{Q}\right)^{(l)} \rightarrow \left(\delta\hat{Q}\right)^{(n)} = \hat{Q}^{(n+1)} - \hat{Q}^{(n)}, \quad m \rightarrow \infty \tag{4}$$

where f denotes an arbitrary quantity, l represents an iteration index and m is an intermediate iteration level between the n-th and the (n+1)-th time levels. The application of the iterative implicit technique to Eq. (1) then yields

$$\left[\frac{\alpha}{\Delta\tau}\delta\hat{Q} + \frac{\partial}{\partial\xi}\left(\delta\hat{E} - \delta\hat{E}_v\right) + \frac{\partial}{\partial\eta}\left(\delta\hat{F} - \delta\hat{F}_v\right)\right]^{(m)} = RHS^{(m)} \tag{5}$$

where $\alpha = 1.5$ and

$$RHS^{(m)} = -\frac{1}{\Delta\tau}\left[\alpha\sum_{l=1}^{m-1}\left(\delta\hat{Q}\right)^{(l)} + (1-\alpha)\left(\delta\hat{Q}\right)^{(n-1)}\right] - \left[\frac{\partial}{\partial\xi}\left(\hat{E} - \hat{E}_v\right) + \frac{\partial}{\partial\eta}\left(\hat{F} - \hat{F}_v\right)\right]^{(m)} \tag{6}$$

Eqs. (5) and (6) represent a Newton-type of timewise linearization on Eq. (1) with $\hat{Q}^{(n+1)}$ as the independent variable. By iterating to convergence, the linearization errors associated with the residuals of the RHS can be driven to zero. Thus, on its convergence, the RHS approaches to a fully implicit nonlinear backward time differencing approximation of the entire unsteady Navier-Stokes equations. The numerical evaluation of the fluxes in Eq. (6) is discussed in Section 3. In the following, the construction of operators approximating the variation of fluxes appearing in the left hand side of Eq. (5) is described.

Associated with each inviscid flux vector, there exists a Jacobian matrix which can be further split into two parts, one is associated with nonnegative eigenvalues and the other with nonpositive eigenvalues. For example,

$$\hat{A}^{+} = \left(\frac{\partial \hat{E}}{\partial \hat{Q}}\right)^{+} \quad , \quad \hat{A}^{-} = \left(\frac{\partial \hat{E}}{\partial \hat{Q}}\right)^{-} \tag{7}$$

are the split Jacobian matrices associated with the flux vector $\hat{E}$. For convenience, the symbol '^' will be dropped from the flow quantities in the subsequent equations and discussion.

By applying the first-order upwind split-flux technique in the context of a Newton-type linearization procedure, the operator approximating the variation of the convective flux is of the following form:

$$\frac{\partial}{\partial \xi}(\delta E)_{i,j} = \frac{1}{\Delta \xi}\left[-\bar{A}^{+}_{i-1,j}(\delta Q)_{i-1,j} + \left(\bar{A}^{+}_{i,j} - \bar{A}^{-}_{i,j}\right)(\delta Q)_{i,j} + \bar{A}^{-}_{i+1,j}(\delta Q)_{i+1,j}\right] \tag{8}$$

In Ref. [3], the matrices $\bar{A}^{+}$ and $\bar{A}^{-}$ are evaluated according to

$$\bar{A}^{+}_{i+1,j} = A^{+}_{i+1,j} \quad , \quad \bar{A}^{-}_{i+1,j} = A^{-}_{i+1,j}$$

and

$$\bar{A}^{+}_{i,j} = A^{+}_{i,j} \quad , \quad \bar{A}^{-}_{i,j} = A^{-}_{i,j} \tag{9}$$

where A^{+} and A^{-} are defined by Eq. (7). In the present work, $\bar{A}^{+}$ and $\bar{A}^{-}$ are evaluated at the Roe-averaged state [4]. For example,

$$\bar{A}^{+}_{i-1,j} = A^{+}(i-1, i; \xi_i) \tag{10a}$$

which means that the flow variables are evaluated at the Roe-averaged state between the nodal points (i-1, j) and (i, j) while the metrics are evaluated at the nodal point (i, j), rather than at the intermediate point (i-1/2,j). The rest of the matrices are evaluated according to

$$\overline{A_{i,j}^{+}} = A^{+}(i-1, i; \xi_i) = \overline{A_{i-1,j}^{+}} \tag{10b}$$

$$\overline{A_{i,j}^{-}} = A^{-}(i, i+1, ; \xi_i) = \overline{A_{i+1,j}^{-}} \tag{10c}$$

The same technique is applied to evaluate $\partial/\partial\eta\,(\delta F)_{i,j}$, in which the associated split matrices are denoted by B^{+} and B^{-}. Thus, the inviscid terms in Eq. (5) yield

$$\frac{\partial}{\partial\xi}(\delta E)_{i,j} + \frac{\partial}{\partial\eta}(\delta F)_{i,j} = [D+L+U](\delta Q)_{i,j} \tag{11}$$

where the operators [D], [L], and [U] are defined as

$$[D](\cdot)_{i,j} = \left(\overline{A_{i,j}^{+}} - \overline{A_{i,j}^{-}} + \overline{B_{i,j}^{+}} - \overline{B_{i,j}^{-}}\right)(\cdot)_{i,j} \tag{12a}$$

$$[L](\cdot)_{i,j} = \left(-\overline{A_{i-1,j}^{+}}\right)(\cdot)_{i-1,j} + \left(-\overline{B_{i,j-1}^{+}}\right)(\cdot)_{i,j-1} \tag{12b}$$

$$[U](\cdot)_{i,j} = \left(\overline{A_{i+1,j}^{-}}\right)(\cdot)_{i+1,j} + \left(\overline{B_{i,j+1}^{-}}\right)(\cdot)_{i,j+1} \tag{12c}$$

The construction of the operator approximating the variation of the viscous fluxes follows the approach of a pointwise Jacobi-iteration

procedure, in which only those parts directly adding terms to the diagonal operator, i.e. Eq. (12a), are retained. The detailed forms of these terms are rather involved and are not shown here. Let V represent the Jacobian of these terms, then, the viscous terms in Eq. (5) yield

$$\frac{\partial}{\partial \xi}(-\delta E_v) + \frac{\partial}{\partial \eta}(-\delta F_v) = [S](\delta Q)_{i,j} \tag{13}$$

where the operator [S] is defined as

$$[S](\cdot)_{i,j} = (V_{i,j})(\cdot)_{i,j} \tag{14}$$

It is further noted here that, if there are external source terms due to, e.g., gravitational acceleration or heat addition, these terms will be, along with $V_{i,j}$, included in the operator [S].

Let I be the identity operator, the evolution process of Eq.(5) is then approximated by

$$[\alpha I + \Delta\tau(S + D + L + U)](\delta Q)_{i,j} = \Delta\tau (RHS)_{i,j} \tag{15}$$

In practice, Eq. (15) is solved by the approximate factorization procedure. In addition, the diagonally-dominant treatment suggested in Ref. [1] is adopted. However, the splitting technique used in the present work is different from that suggested in Ref. [1]. A brief description of the original DDADI algorithm and a demonstration of its numerical instability when the central differencing scheme is used for the inviscid flux terms are given in the Appendix. In the present work, the original splitting technique is modified to enforce the operational symmetry of the factorization. As

demonstrated in the Appendix, this modification renders the overall solution algorithm numerically stable with respect to the central differencing scheme. The presently proposed splitting requires that the temporal iterations are carried out in pairs of advancing steps.

Let $(\delta Q)^l$ denote the solution of the first advancing step and $(\delta Q)^{l+1}$ the solution of the second advancing step of a pair, then $(\delta Q)^l$ at point (i,j) is obtained by solving

$$[\alpha I + \Delta\tau(S + D + L)]\left(\delta Q^*\right)^l_{i,j} = \Delta\tau\,(RHS)^l_{i,j} \tag{16a}$$

$$[\alpha I + \Delta\tau(S + D)]\,(\delta Q)^l_{i,j} = \Delta\tau\,(RHS)^l_{i,j} - [\Delta\tau(L + U)]\left(\delta Q^*\right)^l_{i,j} \tag{16b}$$

and $(\delta Q)^{l+1}_{i,j}$ is obtained by solving

$$[\alpha I + \Delta\tau(S + D + U)]\left(\delta Q^{**}\right)^{l+1}_{i,j} = \Delta\tau\,(RHS)^{l+1}_{i,j} \tag{17a}$$

$$[\alpha I + \Delta\tau(S + D)]\,(\delta Q)^{l+1}_{i,j} = \Delta\tau\,(RHS)^{l+1}_{i,j} - [\Delta\tau(U + L)]\left(\delta Q^{**}\right)^{l+1}_{i,j} \tag{17b}$$

These equations are solved by a pointwise Jacobi-iteration procedure.

The results obtained from several numerical experiments focused on the extra-long time behavior of randomly perturbed uniform background flow suggest that the proposed algorithm would be numerically stable, both in two-and three-dimensional cases, with respect to a variety of differencing schemes described in the following section. It is also noted here that the extension of this LU type of factorization to three-dimensional case is quite

straight forward, no additional sweep is needed to account for the added third dimension.

3. The FCTD Differencing Scheme For The RHS Derivatives

In the past, both central and upwind differencing have been employed to evaluate the RHS spatial derivatives. The third-order-biased upwind scheme (see e.g. Ref.[5]) is the lowest order scheme satisfying the requirement that the leading truncation error is dissipative but not directly contaminating the physically diffusive terms, and it has a stencil of five grid points in each spatial direction. The fourth-order central differencing also has a five-point stencil but the scheme resolution is higher. However, it is non-dissipative by nature, hence allows the excitation of spurious short-wave length modes. In order to suppress these spurious modes, numerical dissipation models (see e.g. [6]) containing fourth-difference dissipation terms are often artificially added to the finite difference equations. These artificial dissipation terms are not consistent with the Navier-Stokes equations. In the following, an analytical way of injecting numerical dissipation to the fourth-order central differencing scheme is presented. For convenience, the index j associated with the η-direction is dropped in the subsequent discussion.

Let $[TU](E)_i$ denote the third-order-biased upwind differencing of the first derivative of E at the spatial point (i,j), then

$$[TU](E)_i = \frac{1}{2h}(E_{i+1} - E_{i-1}) + \frac{1}{6h}(-\Delta E^+_{i-2} + 2\,\Delta E^+_{i-1} - \Delta E^+_i) + \frac{1}{6h}(-\Delta E^-_{i-1} + 2\,\Delta E^-_i - \Delta E^-_{i+1}) \tag{18}$$

where E is the total flux, E^+ and E^- the split fluxes, h = $\Delta\xi$ the grid spacing in computational space and Δ is the forward differencing operator defined as $\Delta(\cdot)_i = (\cdot)_{i+1} - (\cdot)_i$. Under the current effort, the flux-difference splitting suggested by Roe [4] is used in Eq.(18).

A Taylor's series analysis shows that the truncation error associated with the third-order-biased upwind differencing has two parts: a dissipative part (DISS) and a dispersive part (DISP).

$$[TU](E)_i = \left(\frac{\partial E}{\partial \xi}\right)_i + [DISS](E)_i + [DISP](E)_i \tag{19}$$

where

$$[DISS](E)_i = \sum_{l=4,\ \Delta l=2}^{\infty} \frac{1}{3}\left(2^{l-1} - 2\right)\frac{1}{l!}h^{l-1}\frac{\partial^l}{\partial \xi^l}(E^+ - E^-)_i \tag{20}$$

and

$$[DISP](E)_i = \sum_{l=5,\ \Delta l=2}^{\infty} \frac{1}{3}\left(4 - 2^{l-1}\right)\frac{1}{l!}h^{l-1}\left(\frac{\partial^l E}{\partial \xi^l}\right)_i \tag{21}$$

The dissipative part, characterized by the fourth - and higher even - derivatives is given by Eq. (20). The dispersive part, characterized by the fifth - and higher odd - derivatives is given by Eq. (21). It is further noted here that the dissipative part depends on the derivatives of the absolute flux defined as $|E| = E^+ - E^-$, while the dispersive part depends on the derivatives of the total flux.

Let [FC](E)i denote the fourth-order central differencing of the first derivative of E at the spatial point (i,j), then

$$[FC](E)_i = \frac{2}{3}\frac{1}{h}(E_{i+1} - E_{i-1}) - \frac{1}{12}\frac{1}{h}(E_{i+2} - E_{i-2}) \tag{22}$$

It can be shown that

$$[FC](E)_i = \left(\frac{\partial E}{\partial \xi}\right)_i + [DISP]^*(E)_i \tag{23}$$

where

$$[DISP]^*(E)_i = \sum_{l=5,\ \Delta l=2}^{\infty} \frac{1}{3}\left(4 - 2^{l-1}\right)\frac{1}{l!}h^{l-1}\left(\frac{\partial^l E}{\partial \xi^l}\right)_i \tag{24}$$

i.e., the truncation error associated with the fourth-order central differencing is entirely dispersive. By comparing Eq. (24) with Eq. (21), it can be seen that [DISP]*(E)$_i$ is exactly the same as [DISP](E)$_i$. This fact, then, allows the establishment of a working formula for evaluating [DISS](E)$_i$.

Subtracting Eq. (23) from Eq. (19) and using the fact that

$$[DISP]^*(E)_i = [DISP](E)_i \tag{25}$$

the dissipative part of the truncation error is then given by

$$[DISS](E)_i = [TU](E)_i - [FC](E)_i \tag{26}$$

Now that a closed form of [DISS](E)$_i$ becomes available, it can be used to inject numerical dissipation into higher-order central differencing schemes. Here, the scheme under concern is of the fourth-order, and the amended scheme is termed as the fourth-order central differencing with truncation-error- type dissipation (FCTD) scheme. More specifically,

$$[FCTD](E)_i = [FC](E)_i + \beta[DISS](E)_i \tag{27}$$

where β is an adjustable constant. Through Eq. (26), the working formula for FCTD scheme is then

$$[FCTD](E)_i = (1-\beta)[FC](E)_i + \beta[TU](E)_i \tag{28}$$

where $[TU](E)_i$ and $[FC](E)_i$ are given by Eq. (18) and Eq. (22) respectively. Since

$$[FCTD](E)_i = \left(\frac{\partial E}{\partial \xi}\right)_i + \beta[DISS](E)_i + [DISP](E)_i \tag{29}$$

the effective truncation error of the proposed scheme is $\beta[DISS](E)_i + [DISP](E)_i$. It can be seen from Eq. (28) that, when $\beta=0$, FCTD becomes the fourth-order central differencing scheme without numerical dissipation, and, when $\beta=1$, it becomes the third-order-biased upwind scheme.

In a nutshell, the proposed FCTD scheme is an amended fourth-order central differencing scheme with its injected numerical dissipation having the same form as the entire dissipative part of the truncation error intrinsic to the third-order-biased upwind scheme. Such a dissipation is essentially an infinite series with its elements being the fourth - and higher even - derivatives of the absolute flux. The relative amount of added dissipation can be controlled through an adjustable parameter β. It is further noted here that the FCTD scheme yields finite-difference approximations which are consistent with the physical flux derivatives.

In regard to the evaluation of the viscous terms in Eq. (6), these terms are first written in the strong conservation form. Then, half-spacing second-order central differencing scheme is used to evaluate the

derivatives, and simple average is employed to provide mid-point values of transport coefficients. The details of these terms are not shown here.

4. Results - The Convection of a Free Vortex

In references [7,8], the convection of a Lamb-type vortex in a free stream was used as a test case for assessing numerical schemes' ability to preserve and convect concentrated vortices. This test case also is used here to infer the dissipative, dispersive and resolution properties of the proposed scheme.

In test calculations, the reference length is the vortex core radius; the reference flow conditions are the free stream conditions. The number of grid points used is 241 x 61. Figure 1 depicts the computational domain and the grid distribution. In the region containing the vortex path (i.e., $-5 \leq x \leq 50$, $-5 \leq y \leq 5$), the grid spacing is uniform with $\Delta x=\Delta y=0.25$. At t=o, the vortex center is located at the origin (x=o, y=o). The initial condition and the subsequent unsteady boundary conditions are specified through the analytic solution [8] which corresponds to the vortex being convected with a free stream having a Mach number $M_\infty=0.5$. The vortex flow rotates in the clockwise direction. The center pressure (Pc) is a minimum having a value of 0.84. The farfield free stream pressure is $P_\infty=1.0$. The vorticity magnitute of this vortex is shown in Fig.2. The subsequent convection of this vortex is calculated with a constant time step $\Delta t=0.05$, which is used in all the test calculations. These calculations are terminated when the vortex center has traveled a distance of 45 core radii, and this requires a total of 900 time steps. It is further noted here that the advancement of one time step consists of two pairs of Newton-type inner iterations. Based on our experience, this value of the number of

inner iterations represents an optimal use of computer resources for the present problem.

The results obtained by applying the third-order-biased upwind scheme are shown in Figs. 3 and 4. The pattern of vorticity magnitude contours is well preserved, yet there is significant dissipation of vortex strength. It is noted here that the formal accuracy of this scheme is of the third order, and the leading truncation-error term is a dissipative fourth-derivative.

The fourth-order central differencing scheme has the same computational stencil as that of the third-order-biased upwind scheme, but is formally of higher order accuracy. The fourth-order central differencing scheme is intrinsically non-dissipative, and the leading truncation-error term is a dispersive fifth-derivative. Therefore, it can be expected that, without the injection of artificial dissipation, the vortex strength would be better preserved, but spurious short-wave-length components would emerge. These features are demonstrated by results shown in Fig.5 and Fig.6. To suppress the excitation of spurious components, the fourth-difference artificial viscosity model [6] with $\beta^*=0.015$ is used (hereafter, termed as the FCAV scheme), and the results are presented in Figs. 7 and 8. The excitation of phase errors is successfully suppressed during the period of this simulation, and the preservation of the vortex strength is just as good as that shown in Fig. 6. For FCTD scheme, the coefficient of the leading dissipative fourth-derivative term will have a numerical value of 0.015, if β is chosen to be 0.18. Fig. 9 indicates that the vorticity pattern obtained by using the FCTD scheme is well preserved. By comparing Fig. 7(b) and Fig. 9(b), it can be seen that, in Fig. 7(b), there exist incipient short-wave-length components, while the contours in Fig. 9(b) do not exhibit these

spurious components. The results shown in Fig. 10 are slightly more dissipated than those in Fig. 8.

The proposed FCTD scheme with β=0.18 is more accurate than the third-order-biased upwind scheme, but is slightly more dissipative than the FCAV scheme with β^*=0.015. However, the complete absence of spurious short-wave-length components from the contours of vorticity magnitude makes the FCTD differencing a more reliable scheme than the FCAV scheme. The above results are for the case of M_∞=0.5. Flows with M_∞=1.0 and M_∞=1.6 have also been calculated to compare the performances of the schemes in transonic and supersonic regimes. They lead to the same conclusions.

5. Results - The Backward-Facing Step Flows

The application of the proposed algorithm/scheme to the solution of the full Navier-Stokes equations is demonstrated by calculating flows with regions of separation behind a backward-facing step mounted in a two-dimensional channel. The calculated results are then compared with the corresponding experimental data reported in Ref. [9]. This experimental study concluded that, in the laminar range (Re<1200), the flow will maintain its two-dimensionality only when Reynolds number Re<400. The definition of the Reynolds number is given by Re=u(2h)/v, where u is the average inlet velocity, which corresponds to two-thirds of the maximum inlet velocity, h is the height of the inlet channel, and v is the kinematic viscosity. In addition, the channel height downstream of the step is H=1.9423h, and the step height S=0.9423h. Fig. 11 depicts the size of the computational domain and the grid distribution. The number of grid points is 81x31.

Under the current effort, all the calculations were carried out with M_i=0.18 and Pr=0.72, where M_i is the Mach number based on u, and Pr is the laminar Prandtl number. The calculations started with some guessed initial conditions and proceeded until a steady state was reached. The criterion for reaching an asymptotic steady state is that the maximum L_2-norm residual is smaller than $5x10^{-5}$.

Both the fourth-order central differencing with constant-coefficient fourth-difference artificial dissipation (β^*=0.5), i.e. the FCAV scheme, and the proposed FCTD scheme (β=0.5) have been employed to calculate the flows with Reynolds numbers in the laminar range: Re=100, 389, and 1000. The calculated streamwise velocity profiles at stations downstream of the step and their corresponding experimental data are shown in Fig. 12(a) (Re=100), Fig. 12(b) (Re=389), and Fig. 12(c) (Re=1000). For Re=100 and 389, the flows are experimentally two-dimensional, and the present two-dimensional numerical results agree very well with the measured data in terms of the reattachment lengths (shown in table I), and the streamwise velocity profiles (shown in Fig. 12(a) and 12(b)). Furthermore, the results obtained from the two numerical schemes are practically indistinguishable. At Re=1000, the experiment indicated that the flow loses its two-dimensionality. This is reflected in the apparent discrepancies between the experimental data and the two-dimensional numerical results as shown in Fig. 12(c). It is noted here that this kind of discrepancy also exists between the experimental data and two-dimensional numerical results obtained by using other schemes (see e.g. Ref. [9]). It can also be seen that, in the recirculating region, there are some differences between the results obtained from the two numerical schemes. Nevertheless, these differences are considered here as

insignificant.

These two schemes are further compared in terms of the contour plots of the static pressure (Fig. 13 and Fig. 14). For all the practical purposes, the corresponding contour plots can be considered as the same. However, they do reveal some subtle differences in the dissipative features of the two schemes. The FCAV scheme is more effective in smoothing out sharp pressure wiggles associated with the rapid variation of grid spacing in the middle of the larger channel. Although not shown here, it is less effective in damping out the small-amplitude high-wave-number modes of the velocity.

6. Concluding Remarks

The FCTD differencing scheme and an overall solution algorithm have been developed to solve the multi-dimensional unsteady Navier-Stokes equations for compressible flows. The basis of the solution algorithm is a diagonally-dominant approximate factorization procedure. The factorization error and the timewise linearization error associated with this baseline procedure are reduced by performing Newton-type inner iterations at each time step. The robustness of the overall algorithm is enhanced by carrying out the temporal iterations in pairs to enforce the operational symmetry of the factorization procedure. The temporal accuracy is increased to second-order by using the three-point backward time differencing. The viscous fluxes are evaluated by using the half-spacing second-order central differencing scheme. The inviscid fluxes are evaluated by the proposed FCTD scheme, which is an amended fourth-order central differencing scheme with its injected numerical dissipation having the same form as the entire dissipative part of the truncation-error

intrinsic to the third-order-biased upwind scheme. The convection of a free vortex and the backward-facing step flows are chosen as test cases to demonstrate the current capability of this solution algorithm and the FCTD scheme. These numerical results compare well with corresponding analytical solution or experimental data.

Appendix: The DDADI Algorithm and an Investigation of Its Numerical Stability

In terms of the notations used in Eq. (16) and Eq. (17), the DDADI algorithm suggested in Ref.[1] can be written as

$$[\alpha I + \Delta\tau(S+D+L)](\delta Q)^{*} = \Delta\tau(RHS)^{l} \qquad \text{(A1.a)}$$

$$[\alpha I + \Delta\tau(S+D+U)](\delta Q)^{l} = \Delta\tau(RHS)^{l} - [\Delta\tau L](\delta Q)^{*} \qquad \text{(A1.b)}$$

and

$$[\alpha I + \Delta\tau(S+D+U)](\delta Q)^{**} = \Delta\tau(RHS)^{l+1} \qquad \text{(A2.a)}$$

$$[\alpha I + \Delta\tau(S+D+L)](\delta Q)^{l+1} = \Delta\tau(RHS)^{l+1} - [\Delta\tau U](\delta Q)^{**} \qquad \text{(A2.b)}$$

where Eq. (A1) is the counterpart of Eq. (16) and Eq. (A2) is the counterpart of Eq. (17). For convenience, the spatial indices i,j and k have been dropped from these equations. By comparing the respective counterparts, it can be seen that the main difference lies in the treatment of the off-diagonal contributions at the corrector's stage.

A measure of the factorization errors associated with a pair of temporal iterations described by Eqs. (A1) and (A2) is

$$\varepsilon = (\Delta\tau)^{2}\{[L][\alpha I + \Delta\tau(S+D)]^{-1}[U]\}(\delta Q)^{l}$$

$$+ (\Delta\tau)^2\{[U][\alpha I + \Delta\tau(S + D)]^{-1}[L]\}(\delta Q)^{l+1} \qquad \text{(A3)}$$

For the presently proposed algorithm described by Eqs. (16) and(17), a measure of the factorization errors is

$$\begin{aligned}
\varepsilon^* &= -(\Delta\tau)^2[U]\left(\frac{\partial(\delta Q)^*}{\partial\tau}\right) \\
&+ (\Delta\tau)^2\{[L][\alpha I + \Delta\tau(S + D)]^{-1}[U]\}(\delta Q)^* \\
&- (\Delta\tau)^2[L]\left(\frac{\partial(\delta Q)^{**}}{\partial\tau}\right) \\
&+ (\Delta\tau)^2\{[U][\alpha I + \Delta\tau(S + D)]^{-1}[L]\}(\delta Q)^{**}
\end{aligned} \qquad \text{(A4)}$$

Upon the convergence of the temporal iterations, both ε and ε^* are asymptotically removed.

Numerical experiments were conducted to examine the stability characteristics of the original DDADI algorithm and the presently proposed algorithm. In the following, the stability characteristics of these two algorithms when applied to a three-dimensional domain are presented. Fig. A-1 shows the stretched-grid layout of this rectangular domain in a physical space occupied by an inviscid uniform flow with Mach number being 0.35. When the Euler equations are numerically solved to simulate the evolution of this flow, initially broad-band and infinitesimal disturbances originating from the machine round-off error as well as the truncation error associated with the grid stretching will be introduced into the uniform background flow. The subsequent growth of these disturbances is closely related to the numerical stability property of the solution algorithm and differencing scheme. The observed long-time

growth behavior of the disturbances serves to indicate the stability characteristics of the overall solution procedure.

The domain of a 2x1x1 box shown in Fig. A-1 is covered by 21x11x7 grid points, and the background flow is in the x (i.e. I)-direction. The boundary conditions for this investigation are

$$I = 1 \;:\; u = 1,\; v = w = 0,\; T = 1,\; \frac{\partial^2 p}{\partial n^2} = 0$$

$$J = 1,\; K = 1 \;:\; \textit{symmetry conditions}$$

$$I = 21,\; J = 11,\; K = 7 \;:\; \frac{\partial u}{\partial n} = \frac{\partial v}{\partial n} = \frac{\partial w}{\partial n} = \frac{\partial T}{\partial n} = 0,\; p = 1 \qquad \text{(A5)}$$

where n denotes the normal direction.

First-order time-accurate calculations without employing the inner Newton-type iteration process have been conducted. The RHS inviscid flux terms are evaluated with the fourth-order central differencing without any added numerical dissipation. The initial condition is an uniform flow. The time-step used is a constant and has a CFL number of 250. The mid-point, i.e., the point at (I=11, J=6, K=4), is selected as the representative point for illustrating the stability characteristics.

In the case of the original DDADI algorithm [1], the temporal growth of the initially infinitesimal velocity disturbances is depicted in Fig. A-2. It can be seen that, within 2100 time-steps, the disturbances tend to grow out of bounds, and this algorithm is considered as unstable with respect to the fourth-order central differencing scheme under the present test condition.

The solutions at the 2000-th time-step are then used as the initial condition for investigating the stability properties of the presently proposed algorithm. Part of the results are shown in Fig. A-3, which covers a period of the first 4000 time-steps. An additional 16000 time steps have been advanced. Although the entire history of convergence is not shown here, it is clear that converged solutions with the magnitudes of v-component and w-component of the order of10^{-11} are obtained (machine accuracy is of the order of 10^{-13}). The above result suggests that the presently proposed algorithm is numerically stable in three-dimensional domain.

References

1. C. K. LOMBARD, E. VENKATAPATHY, AND J. BARDINA, AIAA paper 84-1533, (1984).

2. M.M. RAI AND S. R. CHAKRAVARTHY, AIAA J. 24, 735 (1986).

3. J. L. STEGER AND R. F. WARMING, J. Comput. Phys. 40, 263 (1981).

4. P. L. ROE, J. Comput. Phys. 43, 357 (1981).

5. B. P. LEONARD, Comput. Methods Appl. Math. Eng. 19, 59 (1979).

6. J. L. STEGER, AIAA J. 16, 679 (1978).

7. M. M. RAI, AIAA paper 87-0543, (1987).

8. N.-S. LIU, F. DAVOUDZADEH, W. R. BRILEY, AND S. J. SHAMROTH, J. Fluids Eng. 112, 501 (1990).

9. B. F. ARMALY, F. DURST, J. C. F. PEREIRA AND B. SCHOENUNG, J. Fluid Mech. 127, 473 (1983).

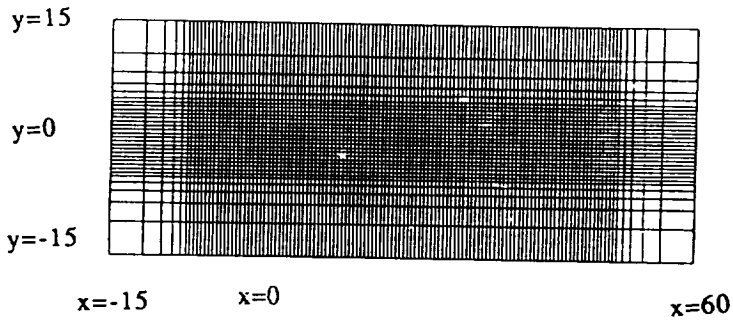

Fig. 1 Computational domain and grid distribution for vortex convection tests (only every other grid lines are shown).

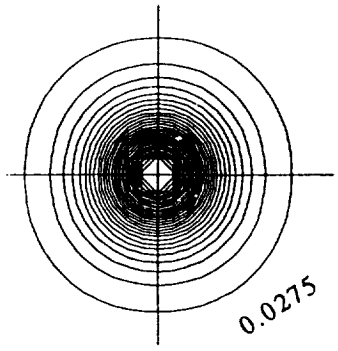

Fig. 2 Contours of the vorticity magnitude (t=0). Increment level=0.0275.

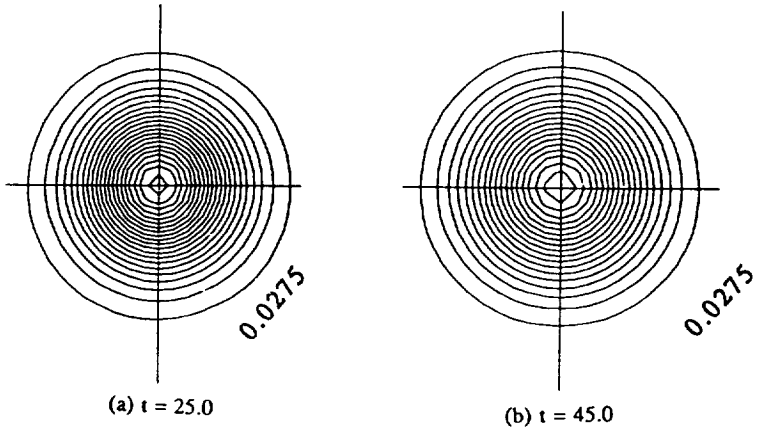

Fig. 3 Contours of the vorticity magnitude (3rd - order - biased upwind differencing). Increment level=0.0275.

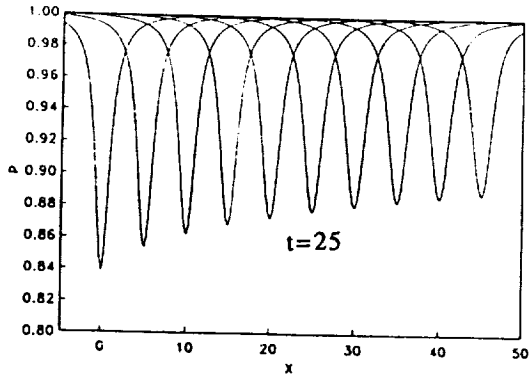

Fig. 4 Static pressure profile along the centerline at different time stations (3rd - order - biased upwind differencing).

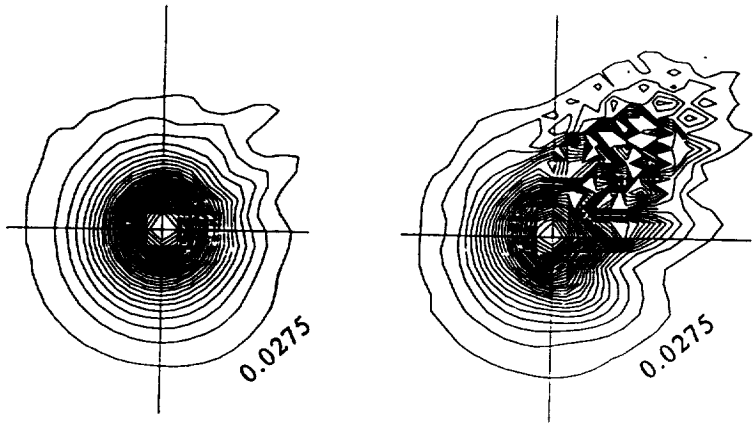

(a) t = 25.0 (b) t = 45.0

Fig. 5 Contours of the vorticity magnitude (4th - order central differencing without artificial dissipation). Increment level=0.0275.

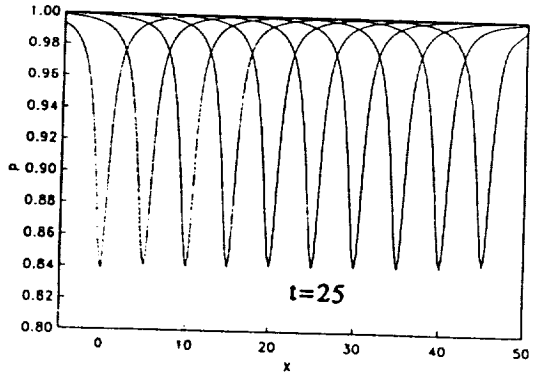

Fig. 6 Static pressure profile along the centerline at different time stations (4th - order central differencing without artificial dissipation).

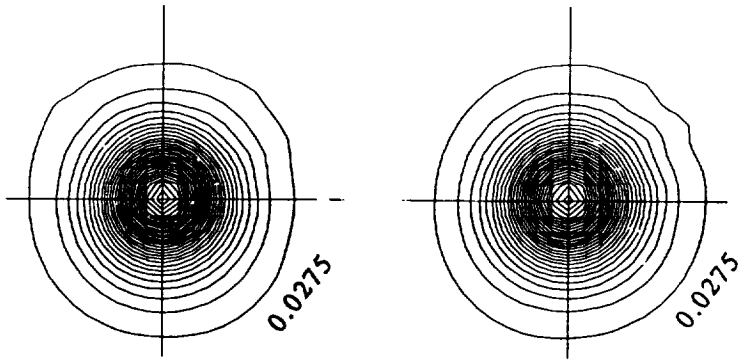

(a) t = 25.0 (b) t = 45.0

Fig. 7 Contours of the vorticity magnitude (FCAV scheme with β^* = 0.015). Increment level=0.0275.

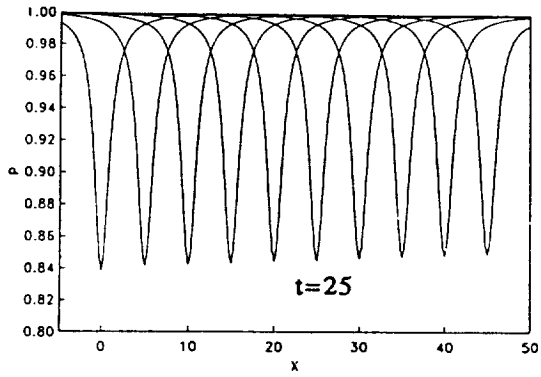

Fig. 8 Static pressure profile along the centerline at different time stations (FCAV scheme with β^* = 0.015).

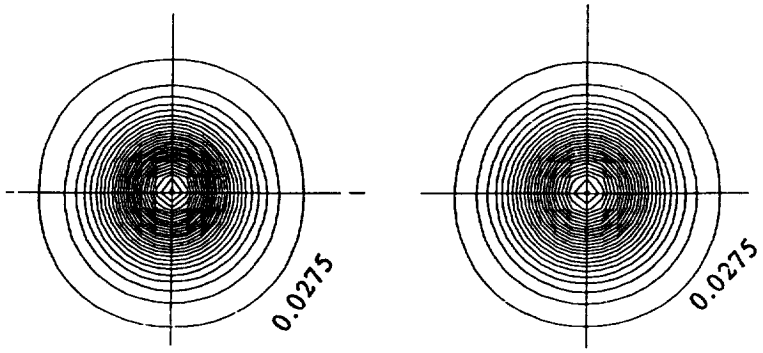

(a) t = 25.0 (b) t = 45.0

Fig. 9 Contours of the vorticity magnitude (FCTD scheme with β = 0.18). Increment level=0.0275

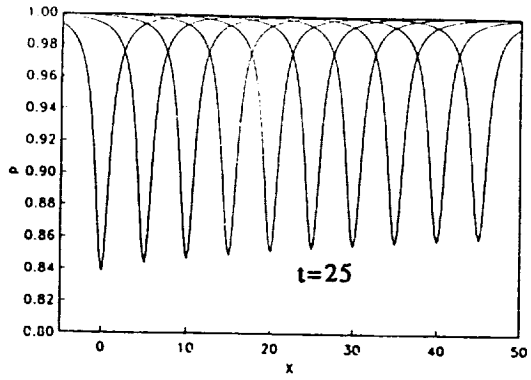

Fig. 10 Static pressure profile along the centerline at different time stations (FCTD scheme with β = 0.18).

Fig. 11 Computational domain and grid distribution for backward-facing step flows (only every other grid lines are shown).

Re	Data	R1	S2	R2
100	FCTD	2.98	-	-
	FCAV	2.94	-	-
	Exp	3.0	-	-
389	FCTD	7.71	-	-
	FCAV	7.60	-	-
	Exp	7.8	-	-
500	FCTD	N.A	N.A	N.A
	FCAV	8.85	7.70	11.70
	Exp	10.0	8.2	13.5
600	FCTD	N.A	N.A	N.A
	FCAV	9.73	8.04	14.10
	Exp	11.2	8.6	14.8
1000	FCTD	11.72	9.23	22.43
	FCAV	12.06	9.46	21.81
	Exp	16.2	13.4	21.8

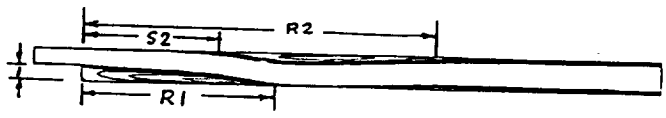

Table I Measured and computed detachment and reattachment length. The flow pattern shown is the contours of streamwise velocity when Re = 1000.

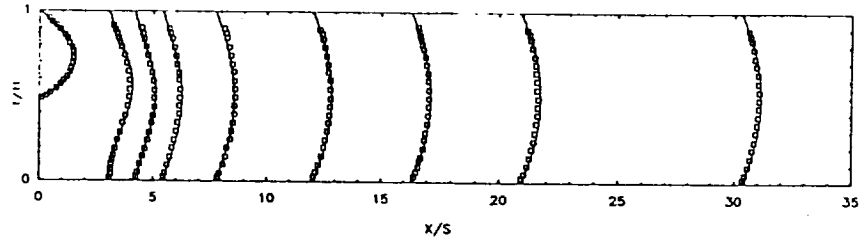

(a) Re = 100

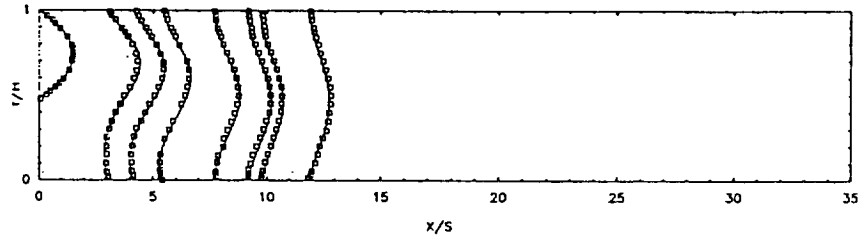

(b) Re = 389

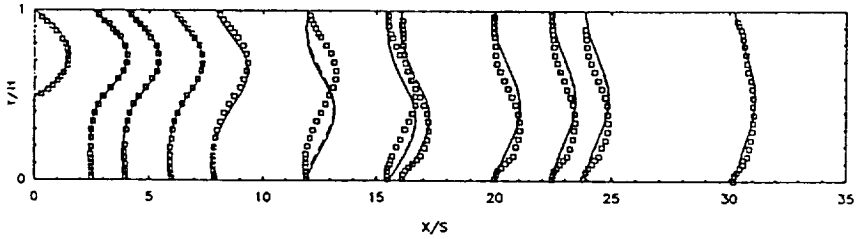

(c) Re = 1000

Fig. 12 Streamwise velocity profiles.

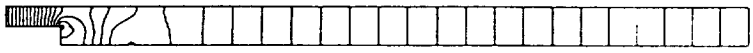

(a) Re = 100

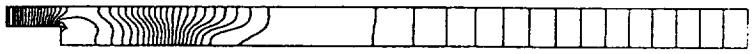

(b) Re = 389

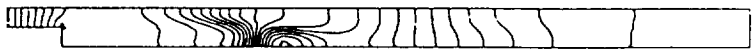

(c) Re = 1000

Fig. 13 Contours of the static pressure (FCTD scheme with β = 0.5).

(a) Re = 100

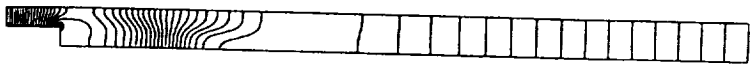

(b) Re = 389

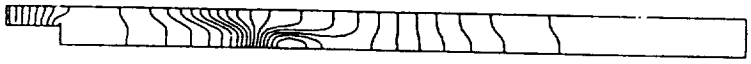

(c) Re = 1000

Fig. 14 Contours of the static pressure (FCAV scheme with $\beta^* = 0.5$).

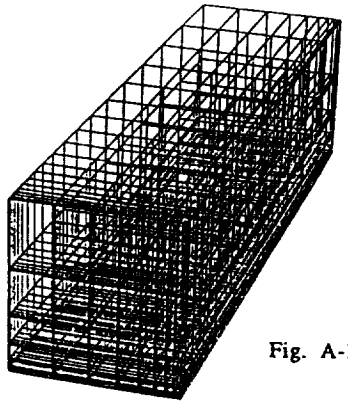

Fig. A-1 Computational domain and grid distribution for test of numerical stability.

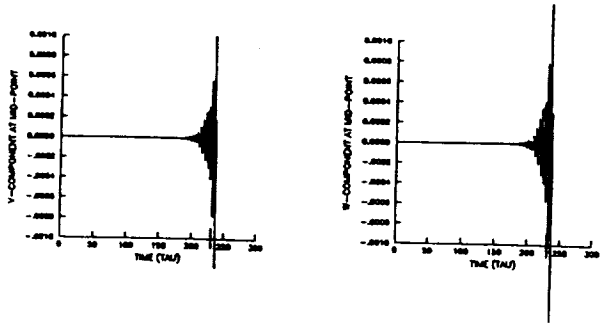

Fig. A-2 Temporal evolution of the velocity disturbance at the mid-point (original DDADI algorithm)

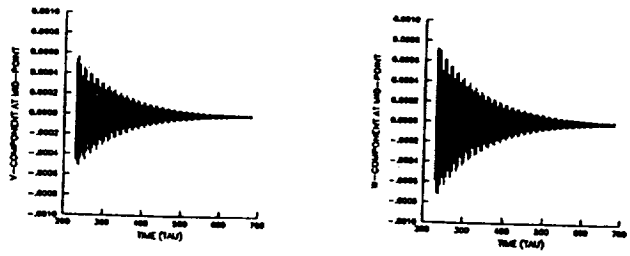

Fig. A-3 Temporal evolution of the velocity disturbance at the mid-point (time-step: 1 - 4000)

REPORT DOCUMENTATION PAGE

Form Approved
OMB No. 0704-0188

1. AGENCY USE ONLY (*Leave blank*)	2. REPORT DATE	3. REPORT TYPE AND DATES COVERED
	October 1991	Technical Memorandum

4. TITLE AND SUBTITLE

An Iterative Implicit Diagonally-Dominant Factorization Algorithm for Solving the Navier-Stokes Equations

5. FUNDING NUMBERS

WU-505-62-52

6. AUTHOR(S)

Shu-Cheng Chen, Nan-Suey Liu, and Hyun Dae Kim

7. PERFORMING ORGANIZATION NAME(S) AND ADDRESS(ES)

National Aeronautics and Space Administration
Lewis Research Center
Cleveland, Ohio 44135-3191

8. PERFORMING ORGANIZATION REPORT NUMBER

E-6589

9. SPONSORING/MONITORING AGENCY NAMES(S) AND ADDRESS(ES)

National Aeronautics and Space Administration
Washington, D.C. 20546-0001

10. SPONSORING/MONITORING AGENCY REPORT NUMBER

NASA TM-105259

11. SUPPLEMENTARY NOTES

Responsible person, Shu-Cheng Chen, (216) 433-8640. The material contained in this report has also been submitted to the Journal of Computational Physics.

12a. DISTRIBUTION/AVAILABILITY STATEMENT

Unclassified - Unlimited
Subject Category 64

12b. DISTRIBUTION CODE

13. ABSTRACT (*Maximum 200 words*)

This paper presents an algorithm for solving the multi-dimensional unsteady Navier-Stokes equations for compressible flows. It is based on a diagonally-dominant approximate factorization procedure. The factorization error and the timewise linearization error associated with this procedure are reduced by performing Newton-type inner iterations at each time step. The inviscid fluxes are evaluated by the fourth-order central differencing scheme amended with a numerical dissipation directly proportional to the entire dissipative part of the truncation error intrinsic to the third-order-biased upwind scheme. The important features of the proposed solution algorithm and the finite-difference scheme are elucidated by the numerical results of the convection of a vortex and the backward-facing step flows.

14. SUBJECT TERMS

Implicit approximate factorization; Intrinsic numerical dissipation; Convection of vortex; Backward-facing step flow

15. NUMBER OF PAGES

30

16. PRICE CODE

A03

17. SECURITY CLASSIFICATION OF REPORT	18. SECURITY CLASSIFICATION OF THIS PAGE	19. SECURITY CLASSIFICATION OF ABSTRACT	20. LIMITATION OF ABSTRACT
Unclassified	Unclassified	Unclassified	